CircSTK39 suppresses the proliferation and invasion in Bladder Cancer via regulating miR-135a-5p/NR3C2-mediated Epithelial-Mesenchymal Transition signaling pathway

Zhi Li
Tianjin Institute of Urology, The Second Hospital of Tianjin Medical University
Zejin Wang
Tianjin Institute of Urology, The Second Hospital of Tianjin Medical University
Shaobo Yang
Tianjin Institute of Urology, The Second Hospital of Tianjin Medical University
Chong Shen
Tianjin Institute of Urology, The Second Hospital of Tianjin Medical University
Yinglang Zhang
Tianjin Institute of Urology, The Second Hospital of Tianjin Medical University
Ruixue Jiang
Tianjin Institute of Urology, The Second Hospital of Tianjin Medical University
Zhe Zhang
Tianjin Institute of Urology, The Second Hospital of Tianjin Medical University
Yu Zhang
Tianjin Institute of Urology, The Second Hospital of Tianjin Medical University
Hailong Hu (hhllove2004@163.com)
Tianjin Institute of Urology, The Second Hospital of Tianjin Medical University

Research Article

Keywords: Circular RNA, bladder cancer, miR-135a-5p, NR3C2, EMT

Posted Date: July 28th, 2022

DOI: https://doi.org/10.21203/rs.3.rs-1867978/v1

Abstract

Circular RNAs (circRNAs), served as a novel non-coding RNA, have crucial functions in the development of tumors, including bladder cancer (BCa). However, the roles and the underlying molecular mechanism of circRNAs mediating epithelial-mesenchymal transition (EMT) processes in BCa remains to be studied. In this research, we first found a novel circRNA, circSTK39 (termed as has_circ_0001079), which was a downregulated gene based on the results of high-throughput RNA sequencing. Subsequently, we determined that the expression of circSTK39 in BCa tissues and their cell lines was significantly reduced. In addition, lower circSTK39 expression was strongly related to a worse prognosis for BCa patients. Next, we detected the biological functions of circSTK39 by using loss- and gain- experiments in vitro and in vivo. Ectopic expression of circSTK39 decreased cell proliferation, colony formation, and invasion capacities, while circSTK39 knockdown prevented the above phenotypes. Mechanically, circSTK39 could sponge with miR-135a-5p, thus inhibiting NR3C2-mediated EMT processes in the BCa progression. In conclusion, our results revealed that circSTK39 inhibited EMT of BCa cells through the miR-135a-5p/NR3C2 axis and may provide promising biomarkers for the diagnosis or prospective therapeutic targets for BCa.

Highlights

- hsa_circ_0001079 is downregulated in BCa and predicts higher likelihood of survival of bladder cancer
- hsa_circ_0001079 overexpression in BCa cells inhibits progression and metastasis of bladder cancer in vitro and in vivo
- hsa_circ_0001079 can regulate NR3C2 expression by competitively interacting with miR-135a-5p, and si-NR3C2 partially revised the biological function of hsa_circ_0001079 in BCa
- hsa_circ_0001079 inhibits the epithelial-mesenchymal transition signaling pathway, and it might be a novel therapeutic target for BCa

1. Introduction

Bladder cancer (BCa) is one of the most diagnosed forms of urinary tumor and carries with it increased morbidity and decreased mortality.(Wong et al. 2018) Although the diagnosis and treatment of BCa have both made rapid progress in recent years, recurrence and metastasis rates remain high. Currently, there are some limitations to the basic research on early diagnosis of BCa in the fields of epigenetics, gene mutations, and metabolomics.(Jacyna et al. 2022;Xue et al. 2021;Piatti et al. 2021) Yet the diagnostic biomarkers from these avenues are still unsatisfactory. Therefore, we set out to uncover novel and more useful biomarkers in order to improve BCa diagnostic strategies.

CircRNAs are a type of non-coding RNA that feature by covalently closed loops.(Wu et al. 2019) Compared to linear RNA, circRNAs lack terminal 5' caps and 3' poly(A) tails and escape RNases digestion, allowing them to be expressed in cells and tissues.(Kristensen et al. 2019;Westholm et al.) Due to their

unique properties, circRNAs play a significant role in the early diagnosis and treatment of many malignant cancers. For example, Zhang et al. utilized RNA sequencing to collect dysregulated circRNA profiles from two pairs of BCa and adjacent tissues, and showed that hsa_circ_0007813 is essential for the development of BCa,(Zhang et al. 2021) and Bi et al. selected downregulated circZKSCAN1 as a research object from circRNAs microarray data and found that it suppressed biological functions in BCa.(Bi et al. 2019) From circRNAs from five pairs of BCa and their adjacent tissues and detected downregulation of has_circ_0077837 and hsa_circ_0004826 in BCa tissues.(Shen et al. 2020) However, the roles and biological processes of circRNAs in BCa remain obscure, particularly in the area of epithelial-mesenchymal transition (EMT).

EMT is a biological process related to the migration, invasion, and metastasis of cancer.(Gaianigo et al. 2017;Zhou et al. 2017) To date, circRNAs have been found to play critical roles in EMT-induced phenotypes of various malignant tumors by regulating EMT transcription factors. For instance, Yang et al. illustrated that circ_0087429 could suppress the development of cervical cancer and EMT via the miR-5003-3p/OGN axis,(Yang et al. 2022) and Yu et al. showed that decreased expression of circ_0092367 promoted gemcitabine resistance and EMT by modulating the miR-1206/ESRP1 axis.(Yu et al. 2021) Though these studies are a good start, more work still needs to be completed to understand the association between circRNAs and EMT in BCa.

In this study, we identified a novel circRNA, has_circ_0001079 (termed circSTK39), whose expression was significantly reduced in BCa tissues and cell lines, using RNA sequencing. Our experiments show that overexpression of circSTK39 decreased the proliferation, colony formation, and invasion capabilities of BCa both in vitro and in vivo. In addition, we also found that circSTK39 may upregulate the mRNA and protein levels of NR3C2, inhibiting EMT-related genes expression at both the transcriptional and post-transcriptional levels. Mechanically, circSTK39, which is mainly located in the cytoplasm of the BCa cells, inhibited BCa EMT by modulating the miR-135a-5p/NR3C2 pathway.

2. Materials And Methods

2.1 Patients Tissue Specimens

For this study we obtained 72 pairs of BCa tissues and matched adjacent nontumor bladder tissues from the Second Hospital of Tianjin Medical University between September 1, 2015 and July 31, 2020. All patients received surgical resection without preoperative radiation or chemotherapy, and were pathologically diagnosed as having BCa. Basic demographics and clinicopathological features were also collected. The Ethics Committee of the Second Hospital of Tianjin Medical University approved this study., and all patients signed the informed consent documents.

2.2 Cell Culture

The BCa cell lines 5637, T24, and EJ were purchased at the Chinese Academy of Sciences Cell bank, and the 253J-BV line was a kind donation from Professor Lei Li of the First Affiliated Hospital of Xian

Jiaotong University. The cells were cultured as previously described.(Shen et al. 2020)

2.3 Cell Transfection

To construct the circSTK39 plasmids used in this study, we cloned the full length of circSTK39 and inserted it into HBLV plasmids (Hanbio, Shanghai, China). Cell lines were transfected by using lentivirus, and stable cell lines were selected and placed in the medium with 0.5 μg/ml puromycin for 7 days. GenePharma (Shanghai, China) designed small interfering RNA (siRNA), miRNA mimics, miRNA inhibitors, and their matching negative controls. Following the manufacturer's instructions, we used Lipofectamine 3000 (Thermo Fisher Scientific, Waltham, USA) to transfect siRNAs and miRNA mimics or inhibitors. All sequences included in the investigation are listed in Table S1.

2.4 Cell Proliferation Assay

To explore changes in proliferation ability, cell counting kit-8 (CCK-8) assay and colony formation assay were applied. For the CCK-8 assay, the pretreated BCa cells were counted and added into a 96-well plate, with a cell concentration of 1.5×10^3 cells/well. The CCK-8 reagent (APExBIO, USA) was then used to detect the optical density at 450 nm after 3 h of incubation at 37°C. For the colony formation experiment, approximately 800 transfected cells per well were planted in six-well plates. After 8–14 days, the cells were fixed in PFA at 4°C and stained with crystal violet at 37°C. Finally, the colonies were counted by hand.

2.5 Wound Healing Assay

A 6-well plate was seeded with 5×10^5 transfected cells that were then grown for 24–48 h until they formed a cell monolayer. Using a 10 μl pipette tip to scratch the cell layer, we then washed each well with PBS and continued culturing with 1640 medium. Photographs of wound healing assay were taken at the same place at 0 and 24 h after scratching.

2.6 Transwell Assay

For the transwell assay 2×10^4 transfected BCa cells were mixed in 200 μl serum-free 1640 medium and were added to the upper chambers covered with 50 μl of matrigel or left uncovered. The bottom chambers were surrounded with 1640 medium containing 20% FBS. After incubation of 24 h for migration and 48 h for invasion, at 37°C, the cells in the lower chambers were fixed in PFA at 4°C, stained with crystal violet at 37°C, photographed, and analyzed by ImageJ software.

2.7 RNA Extraction and Quantitative Real-Time PCR (qRT-PCR)

Total RNA was obtained from tissues and cell lines by following the instructions on the total RNA Kit (Omega, Norcross, USA). Here, 2 μg of total RNA was reverse transcribed to cDNA with the RevertAid First Strand cDNA SynthesisKit (Thermo Fisher Scientific, Waltham, USA). Subsequently, RNA expression levels were determined by qRT-PCR with SYBR Green Premix Ex Taq (Takara, Nanjing, China) on an ABI 7900HT rapid real-time PCR system (Applied Biosystems, Waltham, USA). For circRNAs and mRNAs, we employed

GAPDH as an internal control, and employed U6 as a miRNA internal control. The relative quantitative value of target gene was determined by the $2^{-\Delta\Delta CT}$ method. The sequences of all primers are listed in Table S1.

2.8 Protein Extraction and Western Blot Analysis

Total protein was extracted from cells with a mixture containing RIPA lysis buffer and 1% protease inhibitors, and the protein concentration was measured using a BCA kit (Solarbio, Beijing, China). Equal quantities of 30 μg protein from each sample were separated by 10% SDS–PAGE and then transferred to PVDF membranes (Millipore, USA). The primary antibodies used were as follows, anti-NR3C2 (1:500, ABclonal, Wuhan, China), E-cadherin (1:1000, Cell Signaling Technology, USA), N-cadherin (1:1000, Cell Signaling Technology, USA), Vimentin (1:1000, Cell Signaling Technology, USA), and anti-GAPDH (1:5000, BOSTER, Wuhan, China).

2.9 RNase R Treatment, Actinomycin D Treatment, and Subcellular Fractionation

For RNase R assay, 10 μg total RNA from T24 and 253J-BV were added with or without 20 U/μl RNase R (Abm, Canada) for 2 h at 37℃, and for Actinomycin D assay, T24 and 253J-BV were added with 2 μg/ml Actinomycin D (Sigma, USA) for 0, 4, 8, 12, and 24 h. We used an NE-PERTM kit (Thermo Fisher Scientific, Waltham, USA) to extract cytoplasmic and nuclear fractions according to the manufacturer's instructions and then used qRT-PCR to detect circSTK39, U6, and 18s expression levels. Additionally, U6 and 18s were enriched in the cytoplasm and the nucleus, respectively. The sequences of U6 and 18s primers are listed in Table S1.

2.10 RNA Fluorescence In Situ Hybridization (FISH)

GenePharma (Shanghai, China) developed the Cy3-labeled circSTK39 probe and the FAM-labeled miR-135a-5p probe used for this study. These probes were used to locate circSTK39 and miR-135a-5p in tissues and BCa cell lines, and the probes' sequences are shown in Table S1. The specific steps were carried out according to the manufacturer's protocols for their fluorescence in situ hybridization kit (GenePharma, Shanghai, China). All images were taken by Olympus Confocal Microscope (Olympus, Japan).

2.11 RNA Immunoprecipitation (RIP)

Approximately 1×10^7 T24 cells were harvested in a 15 cm dish and RIP assay was conducted utilizing a RIP kit (BersinBio, Guangzhou, China) and following the manufacturer's instructions. Subsequently, 5 μg of the magnetic bead and the anti-Ago2 (BOSTER, Wuhan, China) or negative control IgG (BOSTER, Wuhan, China) were co-incubated with the cell lysate at 4°C overnight. Both a total RNA Kit and miRNA kit (Omega, Norcross, America) were used to obtain related RNA, and the expression levels of circSTK39 and miR-135-5p were determined using qRT-PCR.

2.12 Biotin-Coupled miRNA Capture

For biotin-coupled capture Approximately 5×10^6 BCa cells (T24 & 253J-BV) were transfected with biotin-miR135a-5p or negative control (NC) by lipofectamine 3000 (Thermo Fisher Scientific, Shanghai, China). After incubation for 24 h, the cells were collected into a 1.5 ml centrifuge tube and then lysed by 500 μl lysis buffer. Subsequently, the cell lysates were incubated with 50 μl of washed streptavidin magnetic beads (Invitrogen) at 4°C for 2 h. Next, the beads were washed and added into 500 μl lysis Buffer (Omega, Norcross, USA). Finally, the expression levels of cricSTK39 and NR3C2 were detected by qRT-PCR analysis.

2.13 Biotin-Coupled CircSTK39 Probe Pull-Down Assay

GenePharma (Shanghai, China) designed biotin-circSTK39 and oligo probes to pull down miRNA. The biotin-circSTK39 and oligo probes were incubated for 2 h at room temperature with washed streptavidin magnetic beads (Invitrogen). Subsequently, 50 μl probe-coated beads were incubated with lysates of 5×10^6 BCa cells at 4°C overnight. After washing, the RNA complexes that had bound to the beads were extracted by 500 μl lysis Buffer (Omega, Norcross, USA), and the expression level of miRNA was analyzed by qRT-PCR assay.

2.14 Dual-Luciferase Reporter Assay

The mutant-type and wild-type circSTK39 reporter plasmids (circSTK39-mut and circSTK39-wt) and NR3C2 mutant-type and wild-type reporter plasmids (NR3C2-mut and NR3C2-wt) were designed by Hanbio (Shanghai, China). The reporter plasmids and miRNA mimics or NC were co-transfected into cells with Lipofectamine 3000, and the activities of both firefly luciferase (LUC) and Renilla luciferase (RLUC) were measured 48 h after transfection using the GloMax® 20/20 Luminometer (Promega, USA) and a Dual-Luciferase Reporter System Kit (Promega, USA). The relative value of luciferase was also calculated for the wild-type and mutant-type groups.

2.15 Xenograft Experiments In Vivo

All animal studies were approved by the Animal Research Ethics Committee of Tianjin Medical University. For in vivo tumor growth studies, 5×10^6 transfected T24 cells mixed in 1:1 PBS/Matrigel solution were subsequently injected into 4-week-old male BALB/C nude mice. Tumor size was measured weekly according to the formula Volume = (long diameter x short diameter^2) ×0.5. The mice were euthanized four weeks after injection, and the tumor tissues were then weighed.

For the metastasis model in vivo, 2×10^6 transfected T24 cells were injected through the tail vein into 4-weeks old BALB/C nude mice. Using the in vivo FX Pro small animal imaging system, fluorescent pictures

of xenografts in nude mice were acquired seven weeks after injection (Brooke company, USA). Both the tumor tissues in THE tumor growth experiment and the lung tumor tissues in the tumor metastasis experiment were fixed in 4% PFA solution and embedded in paraffin.

2.16 IHC

To perform the immunohistochemistry (IHC) assay, the paraffin-embedded tissue sections were incubated with the primary antibody NR3C2 (1:200, ABclonal, Wuhan, China) and Ki-67 (1:1000, Zsbio, Beijing, China) at 4°C overnight. Next, we used anti-IgG secondary antibody (1:200, BOSTER, Wuhan, China) to incubate the sections at 37°C for 1 h. Finally, each section was evaluated by at least two independent pathologists.

2.17 Statistical Analysis

All results that we analyzed came from at least three independently repeated experiments. We used SPSS (IBM, version 21.0.0) and Graphpad prism 8.0 to analyze and visualize the data, respectively, which we transformed into means ± standard deviations (SD). Comparisons between two groups were evaluated using Student's *t* test with two tails, and one-way analysis of variance (ANOVA) was used to examine the differences between the groups. A Kaplan-Meier survival curve was used to describe the OS distribution. Finally, a *p*-value < 0.05 was set as the threshold for statistical significance.

3. Results

3.1 Identification and Characterization of CircSTK39 in BCa

To investigate the role of circRNAs in BCa, we detected the circRNA profiles by RNA sequencing using 5 pairs of BCa and corresponding adjacent tissue. Differently expressed circRNAs were selected under the criteria of |Log2FC|≥2 and p value < 0.05, and the top 40 upregulated and 47 downregulated circRNAs are illustrated in a heatmap and volcano plot (Fig. 1A-B). Among these circRNAs, hsa_circ_0001079 (termed circSTK39) caught our attention. The downregulated expression of circSTK39 was consistent with the RNA sequencing results of GSE97239 (Fig. 1C). CircSTK39 was derived from the exon 2, 3, 4, and 5 regions within the STK39 locus, and its head-to-tail spliced length was 420bp (Fig. 1D). Using qRT-PCR, we further found downregulated expression of circRNAs in BCa cells and 72 pairs of BCa and corresponding adjacent tissue (Fig. 1E-F). Sanger sequencing and random or oligo dT primers were used to test for the presence of circSTK39. Compared to the oligo dT primers, the reverse transcription products using random primers were much higher (Fig. 1G). In addition, convergent primers of circSTK39 were detectable in T24 and 253J-BV cDNA but not gDNA (Fig. 1H). Due to the known stability of circRNAs, we determined that circSTK39 was resistant to RNase R digestion but that STK39 mRNA was diminished (Fig. 1H).

Furthermore, an Actinomycin D work up showed that the half-life of circSTK39 was significantly longer than that of STK39 mRNA in T24 and 253J-BV cells (Fig. 1J). Subsequently, nuclear and cytoplasmic fractions and FISH experiments showed that circSTK39 was abundant in the cytoplasm of both cells and tissues (Fig. 1K-L). To explore the association between the expression of circSTK39 and clinical characteristics of BCa patients further, we collected the survival data and clinical features for each sample. An ROC curve was constructed to assess circ_0001079's potential diagnostic value (Fig. 1M). Table 1 shows that patients with pT2-pT4 had lower expression of circSTK39 (p□0.05), while other clinical characteristics had no significance. Additionally, our Kaplan–Meier curves showed that patients with greater circSTK39 levels had a higher overall survival (OS) rate (Fig. 1N). In addition, univariate and multivariate Cox regression analysis showed that BCa patients with low expression of circSTK39 were independent predictors of OS (Table 2). The above results indicate that circSTK39 was downregulated and may in fact be a biomarker for the development of BCa.

Table1

Correlation between circSTK39 expression and clinicopathologic factors in 72 BCa

Characteristics	Cases (n = 72)	circACVR2A expression		*p* value
		low (n = 36)	high (n = 36)	
Weight(kg)		71.93 ± 12.97	71.33 ± 10.26	
Gender				0.551
Male	58	30	28	
Female	14	6	8	
Age(years)				0.571
≥ 60	16	9	7	
< 60	56	27	29	
History of Smoking				1.000
Ever	40	20	20	
Never	32	16	16	
Pathology stage				0.033*
pTa-pT1	33	12	21	
pT2-pT4	39	24	15	
N stage				0.735
N0	62	30	32	
N1	10	6	4	
M stage				1.000
M0	71	35	36	
M1	1	1	0	
Grade				0.493
Low	2	2	0	
High	70	34	36	
All data are showed as the mean ± SD. *p < 0.05, **p < 0.01, ***p < 0.001				

Table 2
Univariate and multivariate Cox regression analysis of circSTK39 and survival in patients with BCa

Characteristics	Univariate analysis		P value	Multivariate analysis		P value
	HR	95% CI		HR	95% CI	
Age (≥ 60 vs. < 60)	1.008	0.952–1.067	0.793			
Weight (kg)	1.023	0.977–1.070	0.335			
Sex (male vs. female)	0.797	0.176–3.606	0.768			
Grade (low vs. high)	0.540	0.070–4.193	0.556			
Papillary carcinoma (No vs. Yes)	0.950	0.322–2.801	0.926			
History of smoking (No vs. Yes)	0.744	0.267–2.076	0.572			
Carcinoma in situ (absent vs. present)	0.791	0.176–3.548	0.759			
Tumor embolus (absent vs. present)	3.603	1.235–10.513	0.019*	3.077	1.045–9.060	0.041*
Pathological T stage (T1 vs. T2-T4)	2.404	0.763–7.578	0.134			
Pathological N stage (N0 vs. N1)	2.371	0.801–7.023	0.119			
Pathological M stage (M0 vs.M1)	1.647	0.716–15.455	0.66			
circ_0001079 level (high vs. low)	4.341	1.221–15.433	0.023*	3.793	1.059–13.585	0.041*

Abbreviations: HR Hazard ratio, CI Confidence interval, * P < 0.05, **P < 0.01

3.2 The Effects of CircSTK39 on the Proliferation, Migration and Invasion of BCa Cells In Vitro and In Vivo

To investigate the biological impact of circSTK39 on BCa cells, circSTK39 overexpression and a control vector were developed and transfected into 5637, EJ, 253J-BV, and T24 cells. We then conducted qRT-PCR to identify the efficiency of circSTK39 overexpression or knockdown and found that the expression of

circSTK39 was dramatically increased or decreased respectively, while the expression of STK39 mRNA was unaffected (Fig. 2A, Figure S1A-B). Subsequently, wound healing and transwell assays also demonstrated that circSTK39 overexpression could inhibit the migration and invasion abilities of T24 and 253J-BV cells (Fig. 2B-D). However, circSTK39 knockdown restrained the above phenotypes (Figure S1C-D). Furthermore, CCK-8 and colony formation assays demonstrated that circSTK39 overexpression suppressed the viability and cell growth of T24 and 253J-BV cells (Fig. 2E-F), whereas circSTK39 knockdown restrained the above phenotypes (Figure S1E-F). Collectively, these findings suggest that circSTK39 was essential for the in vitro development of BCa cells.

To investigate the biological role of circSTK39 in vivo further, BALB/c nude mice were subcutaneously injected with T24 cells that had been stably transfected with circSTK39 overexpression or a control vector (Fig. 2G). After 4 weeks, we discovered that the tumors in the circSTK39 overexpression group were much smaller and lighter than those in the control vector group (Fig. 2H-I). To detect the expression level of circSTK39 in tumor tissues extracted from xenograft mice, we performed qRT-PCR (Fig. 2J). As shown in Fig. 2K-L, IHC and H&E assays were also performed to detect the expression level of Ki-67, and in addition, we injected T24 cells with circSTK39 overexpression or a control vector into the tail veins of nude mice. After 7 weeks, the luciferase activity of metastatic pulmonary colonies in the circSTK39 overexpression group was considerably lower than in the control vector group (Fig. 2M). We also performed H&E to detect any micro-metastases (Fig. 2N). Collectively, the above findings demonstrated that circSTK39 overexpression inhibited the development and metastasis of BCa in vivo.

3.3 CircSTK39 and Molecular Sponging of miR-135a-5p

Accumulating data suggests that circRNAs may act as sponges to influence downstream genes in BCa. (Yang et al. 2022;Prats et al. 2020) To explore this, we used Starbase, CircInteractome, Circbank, and results of previous studies to predict which miRNAs could bind to circSTK39. Twelve potential miRNAs (miR-135a-5p, miR-135b-5p, miR-1468, miR-581, miR-578, miR-136-5p, miR-633, miR-140-3p, miR-137-3p, miR-137-5p, miR-153-3p, and miR-153-5p) were selected for further experimental validation. To test the interaction between circSTK39 and these twelve potential miRNAs, we performed luciferase reporter assay, anti-AGO2 RIP assay, biotin-coupled miRNA capture assay, biotin-coupled probe pull down assay, and FISH assay.

First, to determine the direct binding site between circSTK39 and it's target miRNAs, HEK-293T cells were transfected with each miRNA mimic and the wild-type circSTK39 reporter plasmid in a luciferase reporter test. The results showed that five miRNAs (miR-135a-5p, miR-135b-5p, miR-1468, miR-581, and miR-578) were able to inhibit luciferase activity significantly (Fig. 3A-B). To make the layout of the binding sites more intuitive, we also designed a diagram of circSTK39 and five potential miRNAs (Fig. 3C). Among them, miR-135a-5p was the most reduced in luciferase activity, by about 60%. To validate the results further, we also co-transfected the mutant circSTK39 reporter plasmid and miR-135a-5p mimics. However, we observed no significant luciferase activity (Figure S2A). Subsequently, we detected the expression level of miR-135a-5p in 23 pairs of BCa and corresponding adjacent tissues, and the results are shown in Fig. 3D.

Second, argonaute2 (AGO2) has a key role in the RNA-induced silencing complex (RISC) that mediates the silencing of miRNA-targets. To this end, our anti-AGO2 RIP assay indicated that circSTK39 and miR-135a-5p were successfully pulled down by the AGO2 antibody compared to IgG antibody as the NC group ($p < 0.01$) (Fig. 3E). Third, in the biotin-coupled probe pull down assay, biotin circSTK39 probe and oligo probe were transfected into T24 and 253J-BV, respectively, to pull down miR-135a-5p (Fig. 3F-G). Additionally, in our biotin-coupled miRNA capture assay, the biotin miR-NC probe and miR-135a-5p probe were transfected into T24 and 253J-BV, respectively, to pull down circSTK39 (Fig. 3H). We conducted qRT-PCR for both of these cases concurrently to validate the interaction between circSTK39 and miR-135a-5p and found that miR-135a-5p was downregulated in circSTK39-overexpressing BCa cells (Fig. 3I). Fourth, in our FISH assay, we observed that cirSTK39 and miR-135a-5p were colocalized in the cytoplasm of BCa cells and tissues (Fig. 3J-K). Collectively, the above results indicated that circSTK39 was able to sponge miR-135a-5p successfully in BCa.

3.4 The Oncogenic Function of MiR-135a-5p in BCa Cells

Recently published studies have reported that miR-135a-5p is an oncogene in several tumors,(Wang et al. 2018;Zhao et al. 2017) including BCa.(Wei et al. 2020;Mao et al. 2015) Our qRT-PCR results revealed that miR-135a-5p was upregulated in BCa cells compared to SV-HUC-1 (Fig. 4A). We also transfected miR-135a-5p mimics or inhibitors into T24 and 253J-BV cells to evaluate their potential biological functions and observed that cell proliferation, migration, and invasion were evidently promoted in these cells (Fig. 4B-F). However, the above phenotypes were also evidently inhibited in T24 and 253J-BV transfected with miR-135a-5p inhibitors (Figure S2B-F). We thus conclude that miR-135a-5p plays a critical role in the progression of BCa.

3.5 MiR-135a-5p Promotes NR3C2-Inudced EMT Processes in BCa Cells.

In order to find the downstream target of circSTK39/miR-135a-5p, we applied bioinformatic tools (Targetscan, miRDB, miRTarbase, and miRwalk) as well as our previous RNA-sequencing results to search for related target genes (Fig. 5A). We analyzed five profiles of predicted potential genes and plotted the heatmap (Figure S3A), and from these NR3C2 caught our attention. Researchers have reported that NR3C2 can be translated into mineralocorticoid receptor (MR), which is a transcription factor that regulates electrolyte balance,(Horisberger and Rossier et al.) and many studies have also reported NR3C2 to be a tumor-suppressing gene and that it suppressed EMT in several types of tumors.(Zhao et al;Zhao et al. 2018) However, whether NR3C2 regulate BCa progression has been unclear.

Initially, our qRT-PCR findings demonstrated that NR3C2 was downregulated in 50 pairs of BCa tissues and cells relative to their respective neighboring tissues and SV-HUC-1(Fig. 5B-C). To increase the credibility of these results, we further tested whether NR3C2 was also downregulated in TCGA samples of BCa and found that it was (Figure S3B). Additionally, we discovered a lower expression of NR3C2 in cancer tissues (T1-T4, N0-N3, M0-M1, or Stage I-Stage IV) compared to paired normal tissues (Figure S3C-F). Moreover, there was decreasing expression of NR3C2 with increasing T stage, and pathologic stage.

However, we observed no statistical difference between T1 stage and normal tissues (Figure S3C). The above results indicate that NR3C2 might be related to the clinical features of BCa.

Next, in the biotin-coupled miRNA capture assay, we also found that the biotin miR-135a-5p probe significantly pulled down NR3C2 mRNA compared to the biotin miR-NC probe (Fig. 5D). Furthermore, we cloned the full length of NR3C2 and inserted it into HBLV plasmids to validate whether miR-135a-5p could directly bind to the 3'-UTR of NR3C2 mRNA, and the results of this experiment showed that miR-135a-5p successfully inhibited luciferase activity (Fig. 5E). After this, in order to confirm the biological functions of NR3C2, we constructed two siRNAs of NR3C2 and transfected them into T24 and 253J-BV. We then performed qRT-PCR to detect the knockdown efficiency of NR3C2 (Fig. 5F) and found that T24 and 253J-BV cells exhibited enhanced proliferation, migration, and invasion after transfection with NR3C2 siRNA (Fig. 5G-K). Finally, after transfection with the circSTK39 overexpression plasmids, qRT-PCR and western blotting validated our findings of altered mRNA and protein expression levels of NR3C2 and EMT-related genes in T24 and 253J-BV (Fig. 6A-C, Figure S3G). After transfection with miR-135a-5p mimics, western blotting also detected the above indices in T24 and 253J-BV (Fig. 6D-E). Hence, we find that NR3C2 is the downstream target of the circSTK39/miR-135a-5p axis and inhibits the progression of BCa.

3.6 CircSTK39 Upregulates NR3C2 Levels and Inhibits EMT via Sponging miR-135a-5p.

To examine further whether circSTK39 regulates cellular biological functions via sponging miR-135a-5p, we designed rescue experiments in BCa cells. These results showed that miR-135a-5p mimics reversed the inhibitory function of circSTK39 on the proliferation, migration, and invasion abilities of T24 and 253J-BV (Fig. 6F-G, Figure S4A-C). Additionally, to test whether circSTK39 inhibited the BCa progression via altering NR3C2, we also designed rescue experiments for the above functional experiments, and these experimental results indicated that NR3C2 knockdown obtained the same phenotype (Fig. 7A-B, Figure S4D-F). Afterwards, western blot showed that NR3C2 was connected to EMT-related genes (Fig. 7C-D). Moreover, after transfection with circSTK39 plasmids, we validated at the protein level that miR-135a-5p mimics or NR3C2 knockdown could partially rescue the expression of NR3C2 in T24 and 253J-BV (Fig. 7E-H). Finally, the association between circSTK39 and NR3C2 in vivo was further tested by qRT-PCR and IHC in order to detect the expression level of NR3C2 in tumor tissues extracted from xenograft mice (Fig. 8A-B). All of the above results taken together indicate that circSTK39 suppresses NR3C2-induced BCa EMT by sponging miR-135a-5p.

4. Discussion

Growing evidence has supported the idea that circRNAs possess the features of high sequence conservation, high stability, and tissue specificity.(Wilusz et al. 2018;Salzman et al.) Currently, many studies have reported that circRNAs may be able to serve as novel biomarkers for cancer diagnosis and prognosis, including for BCa. For instance, Li et al. found that upregulated circ_00141130 in BCa could enhance tumor development through the miR-132-3p/KCNJ12 axis,(Li et al. 2021) and Dong et al.

reported that circ_0001073 could sponge with miR-626 to inhibit BCa proliferation and metastasis further. (Dong et al. 2019) Similarly, Jin et al. found that circ_0001944 was closely correlated to BCa occurrence and regulated BCa growth through the miR-548/PROK2 axis.(Jin et al. 2020)

In our present study, we found circSTK39 to be a circRNA with a longer half-life and resistance to RNase R digestion compared to STK39 mRNA. Furthermore, we detected downregulated circSTK39 detected in 72 pairs of BCa and corresponding adjacent tissues. We used a series of in vitro and in vivo functional tests to come to the conclusion that circSTK39 suppressed the proliferation, migration, and invasion of BCa cells, and decreased tumor size and weight. Moreover, we found that decreased circSTK39 expression was closely correlated with advanced TNM stage and shorter OS rate. Our univariate and multivariate Cox regression analysis also validated the independent predictive power of circSTK39. The preceding investigations all suggest that circSTK39 may contribute to the evolution of BCa.

Previous studies have reported that circRNAs exert biological functions through many pathways, including miRNA sponges, RNA-binding protein sponges, transcriptional factors, and proteins translation. (Yang et al. 2022;Prats et al. 2020;Yang et al. 2019;Lu et al. 2019;Wu et al. 2019) Among these functions, the best-known is that circRNAs primarily sponge miRNAs to regulate target mRNA genes. Sun et al. for instance found that circ_0062682 promoted growth in colorectal cancer by serving as a competitive endogenous RNA for miR-940,(Sun et al. 2021) and Zang et al. illustrated that circ_0000337 could accelerate the cisplatin resistance of esophageal cancer and regulate JAK2 expression by competitively interacting with miR-337-3p.(Zang et al. 2021) Concordantly, at the beginning of our mechanism exploration, RIP assay and RNA pull down assay were designed to validate the existence of miRNA sponge. Next, to find the potential target miRNAs of circSTK39, we considered the results of bioinformatic analysis and of previous research. We selected MiR-135a-5p and regarded it as an oncogene in BCa.

Along these lines Mao et al. found that miR-135a-5p could downregulate the expression of GSK3β to promote the EMT, invasion, and migration of BCa,(Mao et al. 2018) and Wei et al. and Mao et al. also reported that upregulated miR-135a-5p could enhance cellular proliferation in BCa.(Wei et al. 2020;Mao et al. 2015) To test the above theory, we measured the differential expression of miR-135a-5p in BCa tissues and cells. Our FISH assay showed that circSTK39 was co-localized with miR-135-5p, and luciferase reporter assay further identified the binding site directly. Finally, our in vivo experiments indicated that miR-135a-5p facilitated the proliferation, migration, and invasion of BCa cells by triggering EMT. According to our rescue experiments, miR-135a-5p was able to partially reverse the inhibitory effect of circSTK39. With all of its results taken together, our study identified the regulation relationship between circSTK39 and miR-135a-5p.

Matured miRNA has been found to be an important component of RISCs that can decrease the expression of target genes by binding to the 3’UTR of downstream mRNAs.(Bartel et al. 2018;Jonas and Izaurralde et al. 2015) In this vein we analyzed the results from bioinformatics analysis and RNA sequencing and selected NR3C2 as the downstream target gene of circSTK39/miR-135a-5p. The NR3C2 gene is a member of nuclear receptor subfamily 3 group C and has been reported as a tumor suppressor

in multiple cancers. For example, Peng et al. and Fan et al. found that NR3C2 overexpression is positively correlated to poor overall survival (OS) for breast cancer and could also be a prognosis marker.(Fan et al. 2021;Peng et al. 2021) In addition, NR3C2, as a transcription factor, has been shown to be downregulated in and to inhibit the malignant phenotypes of glioblastoma and pancreatic cancer.(Zhao et al. 2020;Yang et al. 2016) However, the role of NR3C2 had yet to be elucidated in BCa.

In this study, we found that NR3C2 was downregulated in 50 pairs of BCa samples and TCGA samples, which was consistent with the above findings for other cancers. Moreover, we observed a positive correlation between decreased NR3C2 expression and poor clinical outcomes of patients with BCa. As mentioned previously, NR3C2 is regarded as a tumor suppressor and an inhibitor of EMT process in other cancers. For example, Zhao et al. found that NR3C2 overexpression could decrease EMT expression and reduce clear-cell renal carcinoma growth. In 2017,(Zhao et al. 2018) and Zhang et al. found that NR3C2 was the target gene of miR-135b-5p and that it inhibited the EMT of pancreatic cancer cells. In this paper we demonstrated that NR3C2 knockdown could increase BCa cells' malignant phenotypes and EMT by qRT-PCR and western blot analysis.(Zhang et al. 2017) Subsequently, our luciferase reporter and RNA pull-down assay showed that miR-135a-5p could directly bind to the 3'-UTR of NR3C2, our rescue experiments showed that NR3C2 knockdown could partially reverse the inhibitory impact of circSTK39. Furthermore, our correlation analysis showed that in BCa tissues, NR3C2 expression was positively correlated with circSTK39 expression but negatively correlated with miR-135a-5p expression.

5. Conclusion

In summary, our study demonstrated that circSTK39 was downregulated in BCa and that it plays and played a tumor suppressing role. Additionally, lower expression of circSTK39 was significantly associated with the worse clinicopathological features of BCa patients. Mechanism analysis showed that circSTK39 increased NR3C2 expression by sponging miR-135a-5p to modulate the EMT pathway of BCa (Fig. 8C). Therefore, our results indicate that circSTK39 is a promising biomarker for the diagnosis and prognosis of BCa patients.

Declarations

Acknowledgments The authors thank AiMi Academic Services (www.aimieditor.com) for the English language editing and review services.The present study received financial support from the Natural Science Foundation Project of Tianjin (grant no. 18PTLCSY00010), the Tianjin Urological Key Laboratory Foundation (grant no. 2017ZDSYS13) and the Youth Fund of Tianjin Medical University Second Hospital (grant no. 2020ydey09).

Data availability All data generated or analysed during this study are included in this published article and its supplementary information files.

Autor contribution Zhi li, Zejin Wang and Shaobo Yang performed the experiments and generated data. Chong Shen, Yinglang Zhang, Runxue Jiang and Zhe Zhang analyzed data. Zhi li, Zejin Wang and Shaobo Yang designed the experiments. Zhi li wrote the manoscript. Hailong Hu revised the manuscript. All authors contributed to the article. All authors read and approved the final manuscript.

Funding The present study received financial support from the Natural Science Foundation Project of Tianjin (grant no. 18PTLCSY00010), the Tianjin Urological Key Laboratory Foundation (grant no. 2017ZDSYS13) and the Youth Fund of Tianjin Medical University Second Hospital (grant no. 2020ydey09).

Competing interests The authors declare no competing interests.

Ethics approval The present study was approved by the Ethics Committee of the second Hospital of Tianjin Medical University (NO.KY2020K063).

Consent to participate Participants were asked to sign informed consent before using clinical resources.

Consent for publication All of the authors are aware of and agree to the content of the paper and their being listed as a co-author of the paper.

References

1. Wong MCS, Fung FDH, Leung C, Cheung WWL, Goggins WB, Ng CF. The global epidemiology of bladder cancer: a joinpoint regression analysis of its incidence and mortality trends and projection. Scientific Reports. 2018;8(1):1129.http://doi.org/10.1038/s41598-018-19199-z
2. Jacyna J, Kordalewska M, Artymowicz M, Markuszewski M, Matuszewski M, Markuszewski MJ. Pre- and Post-Resection Urine Metabolic Profiles of Bladder Cancer Patients: Results of Preliminary Studies on Time Series Metabolomics Analysis. Cancers. 2022;14(5).http://doi.org/10.3390/cancers14051210
3. Xue C, Chen X, Lin K, Tong Y, Wang X. Identification of Notch signaling pathway gene mutations as a prognostic biomarker for bladder cancer. Future Oncology. 2021;17(32):4307–20.http://doi.org/10.2217/fon-2021-0110
4. Piatti P, Chew YC, Suwoto M, Yamada T, Jara B, Jia X-Y, et al. Clinical evaluation of Bladder CARE, a new epigenetic test for bladder cancer detection in urine samples. Clinical Epigenetics. 2021;13(1):84.http://doi.org/10.1186/s13148-021-01029-1
5. Wu J, Qi X, Liu L, Hu X, Liu J, Yang J, et al. Emerging Epigenetic Regulation of Circular RNAs in Human Cancer. Molecular Therapy - Nucleic Acids. 2019;16:589 – 96.http://doi.org/10.1016/j.omtn.2019.04.011
6. Kristensen LS, Andersen MS, Stagsted LVW, Ebbesen KK, Hansen TB, Kjems J. The biogenesis, biology and characterization of circular RNAs. Nature Reviews Genetics. 2019;20(11):675 – 91.http://doi.org/10.1038/s41576-019-0158-7

7. Westholm JO, Miura P, Olson S, Shenker S, Joseph B, Sanfilippo P, et al. Genome-wide analysis of drosophila circular RNAs reveals their structural and sequence properties and age-dependent neural accumulation. (2211 – 1247 (Electronic))
8. Zhang Z, Mou Z, Xu C, Wu S, Dai X, Chen X, et al. Autophagy-associated circular RNA hsa_circ_0007813 modulates human bladder cancer progression via hsa-miR-361-3p/IGF2R regulation. Cell Death & Disease. 2021;12(8):778.http://doi.org/10.1038/s41419-021-04053-4
9. Bi J, Liu H, Dong W, Xie W, He Q, Cai Z, et al. Circular RNA circ-ZKSCAN1 inhibits bladder cancer progression through miR-1178-3p/p21 axis and acts as a prognostic factor of recurrence. Molecular Cancer. 2019;18(1):133.http://doi.org/10.1186/s12943-019-1060-9
10. Shen C, Wu Z, Wang Y, Gao S, Da L, Xie L, et al. Downregulated hsa_circ_0077837 and hsa_circ_0004826, facilitate bladder cancer progression and predict poor prognosis for bladder cancer patients. Cancer Medicine. 2020;9(11):3885 – 903.http://doi.org/10.1002/cam4.3006
11. Gaianigo N, Melisi D, Carbone C. EMT and Treatment Resistance in Pancreatic Cancer. Cancers. 2017;9(9).http://doi.org/10.3390/cancers9090122
12. Zhou P, Li B, Liu F, Zhang M, Wang Q, Liu Y, et al. The epithelial to mesenchymal transition (EMT) and cancer stem cells: implication for treatment resistance in pancreatic cancer. Molecular Cancer. 2017;16(1):52.http://doi.org/10.1186/s12943-017-0624-9
13. Yang M, Hu H, Wu S, Ding J, Yin B, Huang B, et al. EIF4A3-regulated circ_0087429 can reverse EMT and inhibit the progression of cervical cancer via miR-5003-3p-dependent upregulation of OGN expression. Journal of Experimental & Clinical Cancer Research. 2022;41(1):165.http://doi.org/10.1186/s13046-022-02368-4
14. Yu S, Wang M, Zhang H, Guo X, Qin R. Circ_0092367 Inhibits EMT and Gemcitabine Resistance in Pancreatic Cancer via Regulating the miR-1206/ESRP1 Axis. Genes. 2021;12(11).http://doi.org/10.3390/genes12111701
15. Prats A-C, David F, Diallo LH, Roussel E, Tatin F, Garmy-Susini B, et al. Circular RNA, the Key for Translation. International Journal of Molecular Sciences. 2020;21(22).http://doi.org/10.3390/ijms21228591
16. Wang LX, Kang ZP, Yang ZC, Ma RX, Tan Y, Peng XB, et al. MicroRNA-135a Inhibits Nasopharyngeal Carcinoma Cell Proliferation Through Targeting Interleukin-17. Cellular Physiology and Biochemistry. 2018;46(6):2232–8.http://doi.org/10.1159/000489591
17. Zhao X, Sun Z, Li H, Jiang F, Zhou J, Zhang L. MiR-135a-5p modulates biological functions of thyroid carcinoma cells via targeting VCAN 3'-UTR. Cancer Biomarkers. 2017;20:207 – 16.http://doi.org/10.3233/CBM-170566
18. Wei X, Yang X, Wang B, Yang Y, Fang Z, Yi C, et al. LncRNA MBNL1-AS1 represses cell proliferation and enhances cell apoptosis via targeting miR-135a-5p/PHLPP2/FOXO1 axis in bladder cancer. Cancer Medicine. 2020;9(2):724 – 36.http://doi.org/10.1002/cam4.2684
19. Mao XP, Zhang LS, Huang B, Zhou SY, Liao J, Chen LW, et al. Mir-135a enhances cellular proliferation through post-transcriptionally regulating PHLPP2 and FOXO1 in human bladder cancer. Journal of

Translational Medicine. 2015;13(1):86.http://doi.org/10.1186/s12967-015-0438-8

20. Horisberger JD, Rossier BC. Aldosterone regulation of gene transcription leading to control of ion transport. (0194-911X (Print))
21. Zhao R, Ni J, Lu S, Jiang S, You L, Liu H, et al. CircUBAP2-mediated competing endogenous RNA network modulates tumorigenesis in pancreatic adenocarcinoma. (1945–4589 (Electronic))
22. Zhao Z, Zhang M, Duan X, Deng T, Qiu H, Zeng G. Low NR3C2 levels correlate with aggressive features and poor prognosis in non-distant metastatic clear-cell renal cell carcinoma. Journal of Cellular Physiology. 2018;233(10):6825–38.http://doi.org/10.1002/jcp.26550
23. Wilusz JE. A 360° view of circular RNAs: From biogenesis to functions. WIREs RNA. 2018;9(4):e1478.http://doi.org/10.1002/wrna.1478
24. Salzman J, Chen Re Fau - Olsen MN, Olsen Mn Fau - Wang PL, Wang Pl Fau - Brown PO, Brown PO. Cell-type specific features of circular RNA expression. (1553–7404 (Electronic))
25. Li G, Guo B-y, Wang H-d, Lin G-t, Lan T-j, Ying H, et al. CircRNA hsa_circ_0014130 function as a miR-132-3p sponge for playing oncogenic roles in bladder cancer via upregulating KCNJ12 expression. Cell Biology and Toxicology. 2021.http://doi.org/10.1007/s10565-021-09668-z
26. Dong W, Bi J, Liu H, Yan D, He Q, Zhou Q, et al. Circular RNA ACVR2A suppresses bladder cancer cells proliferation and metastasis through miR-626/EYA4 axis. Molecular Cancer. 2019;18(1):95.http://doi.org/10.1186/s12943-019-1025-z
27. Jin M, Lu S, Wu Y, Yang C, Shi C, Wang Y, et al. Hsa_circ_0001944 promotes the growth and metastasis in bladder cancer cells by acting as a competitive endogenous RNA for miR-548. Journal of Experimental & Clinical Cancer Research. 2020;39(1):186.http://doi.org/10.1186/s13046-020-01697-6
28. Yang F, Hu A, Li D, Wang J, Guo Y, Liu Y, et al. Circ-HuR suppresses HuR expression and gastric cancer progression by inhibiting CNBP transactivation. Molecular Cancer. 2019;18(1):158.http://doi.org/10.1186/s12943-019-1094-z
29. Lu Q, Liu T, Feng H, Yang R, Zhao X, Chen W, et al. Circular RNA circSLC8A1 acts as a sponge of miR-130b/miR-494 in suppressing bladder cancer progression via regulating PTEN. Molecular Cancer. 2019;18(1):111.http://doi.org/10.1186/s12943-019-1040-0
30. Wu N, Yuan Z, Du KY, Fang L, Lyu J, Zhang C, et al. Translation of yes-associated protein (YAP) was antagonized by its circular RNA via suppressing the assembly of the translation initiation machinery. Cell Death & Differentiation. 2019;26(12):2758–73.http://doi.org/10.1038/s41418-019-0337-2
31. Sun S, Li C, Cui K, Liu B, Zhou M, Cao Y, et al. Hsa_circ_0062682 Promotes Serine Metabolism and Tumor Growth in Colorectal Cancer by Regulating the miR-940/PHGDH Axis. Front Cell Dev Biol. 2021
32. Zang R, Qiu X, Song Y, Wang Y. Exosomes Mediated Transfer of Circ_0000337 Contributes to Cisplatin (CDDP) Resistance of Esophageal Cancer by Regulating JAK2 via miR-377-3p. Frontiers in Cell and Developmental Biology. 2021;9

33. Mao X-W, Xiao J-Q, Li Z-Y, Zheng Y-C, Zhang N. Effects of microRNA-135a on the epithelial–mesenchymal transition, migration and invasion of bladder cancer cells by targeting GSK3β through the Wnt/β-catenin signaling pathway. Experimental & Molecular Medicine. 2018;50(1):e429-e.http://doi.org/10.1038/emm.2017.239
34. Bartel DP. Metazoan MicroRNAs. Cell. 2018;173(1):20–51.http://doi.org/10.1016/j.cell.2018.03.006
35. Jonas S, Izaurralde E. Towards a molecular understanding of microRNA-mediated gene silencing. Nature Reviews Genetics. 2015;16(7):421–33.http://doi.org/10.1038/nrg3965
36. Fan Y, Li Y, Zhu Y, Dai G, Wu D, Gao Z, et al. miR-301b-3p Regulates Breast Cancer Cell Proliferation, Migration, and Invasion by Targeting NR3C2. Journal of Oncology. 2021;2021:8810517.http://doi.org/10.1155/2021/8810517
37. Peng Y, Xi X, Li J, Ni J, Yang H, Wen C, et al. miR-301b and NR3C2 co-regulate cells malignant properties and have the potential to be independent prognostic factors in breast cancer. Journal of Biochemical and Molecular Toxicology. 2021;35(2):e22650.http://doi.org/10.1002/jbt.22650
38. Zhao X, Shen F, Ma J, Zhao S, Meng L, Wang X, et al. CREB1-induced miR-1204 promoted malignant phenotype of glioblastoma through targeting NR3C2. Cancer Cell International. 2020;20(1):111.http://doi.org/10.1186/s12935-020-01176-0
39. Yang S, He P, Wang J, Schetter A, Tang W, Funamizu N, et al. A Novel MIF Signaling Pathway Drives the Malignant Character of Pancreatic Cancer by Targeting NR3C2. Cancer Research. 2016;76(13):3838–50.http://doi.org/10.1158/0008-5472.CAN-15-2841
40. Zhang Z, Che X, Yang N, Bai Z, Wu Y, Zhao L, et al. miR-135b-5p Promotes migration, invasion and EMT of pancreatic cancer cells by targeting NR3C2. Biomedicine & Pharmacotherapy. 2017;96:1341–8.http://doi.org/10.1016/j.biopha.2017.11.074

Figures

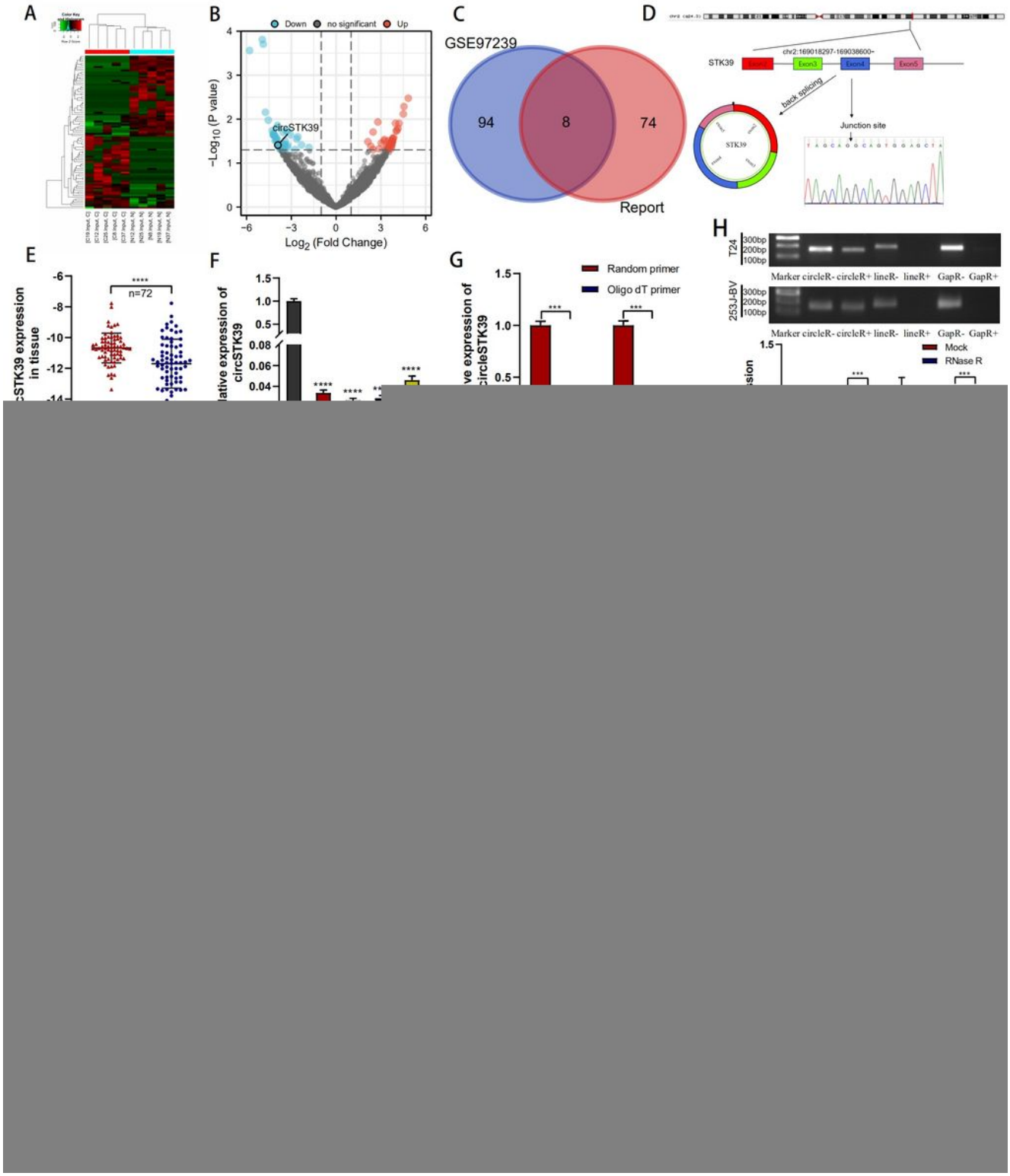

Figure 1

CircSTK39 expression is downregulated in bladder cancer cells and tissues

(A-B) The heatmap plots and volcano plots showed the dysregulated circRNAs in 5 pairs of bladder cancer tissues and corresponding adjacent tissues. The red designates up-regulated and green represents down-regulated.

(C) The intersection of GSE97239 dataset and 5 pairs BCa sequencing results.

(D) Schematic illustration of circSTK39 formation via the circularization from exons 2 to exons 5 in STK39 gene. Sanger sequencing is used to verify the existence of circSTK39. The black arrows represent its back splicing junction

(E) circSTK39 expression was measured using qRT-PCR in 72 pairs of primary bladder cancer tissues and adjacent normal samples.

(F) circSTK39 expression was measured using qRT-PCR in SV-HUC-1 and bladder cancer cells.

(G) Either oligo-dT primer or random primer were used to obtain the reverse-transcribed RNA in T24 and 253J-BV cells.

(H) After RNase R treatment, the expression of circSTK39, STK39, and GAPDH in T24 and 253J-BV were detected by qRT-PCR.

(I) Both divergent and convergent primers were designed to prove the existence of circSTK39 in T24 and 253J-BV cell lines by RT-PCR. cDNA and gDNA were used as the template for verification. GAPDH and STK39 mRNA were used as negative control.

(J) After actinomycin D treatment, the expression of circSTK39, STK39, and GAPDH in T24 and 253J-BV were detected by qRT-PCR.

(K) The intracellular localization of circSTK39 was also evaluated in bladder tissues (magnification, × 600, Scale bar, 50 μm) and cells (magnification, × 400, Scale bar, 50 μm) by FISH. circSTK39 probe was tagged with cy3, and nuclei were stained with DAPI.

(L) Nuclear-cytoplasmic fractionation assay was performed to measure the expression of circSTK39 in T24 and 253J-BV cells.18s was considered as a cytoplasmic protein control and U6 was used as a nuclear control.

(M) The ROC curve has been performed to assess circ_0001079 potential diagnostic value.

(N) Kaplan–Meier curves showed the association between the higher circSTK39 levels and the longer overall survival rate.

Data were shown as mean ± SD, n = 3 *P < 0.05, **P < 0.01, ***P < 0.001.

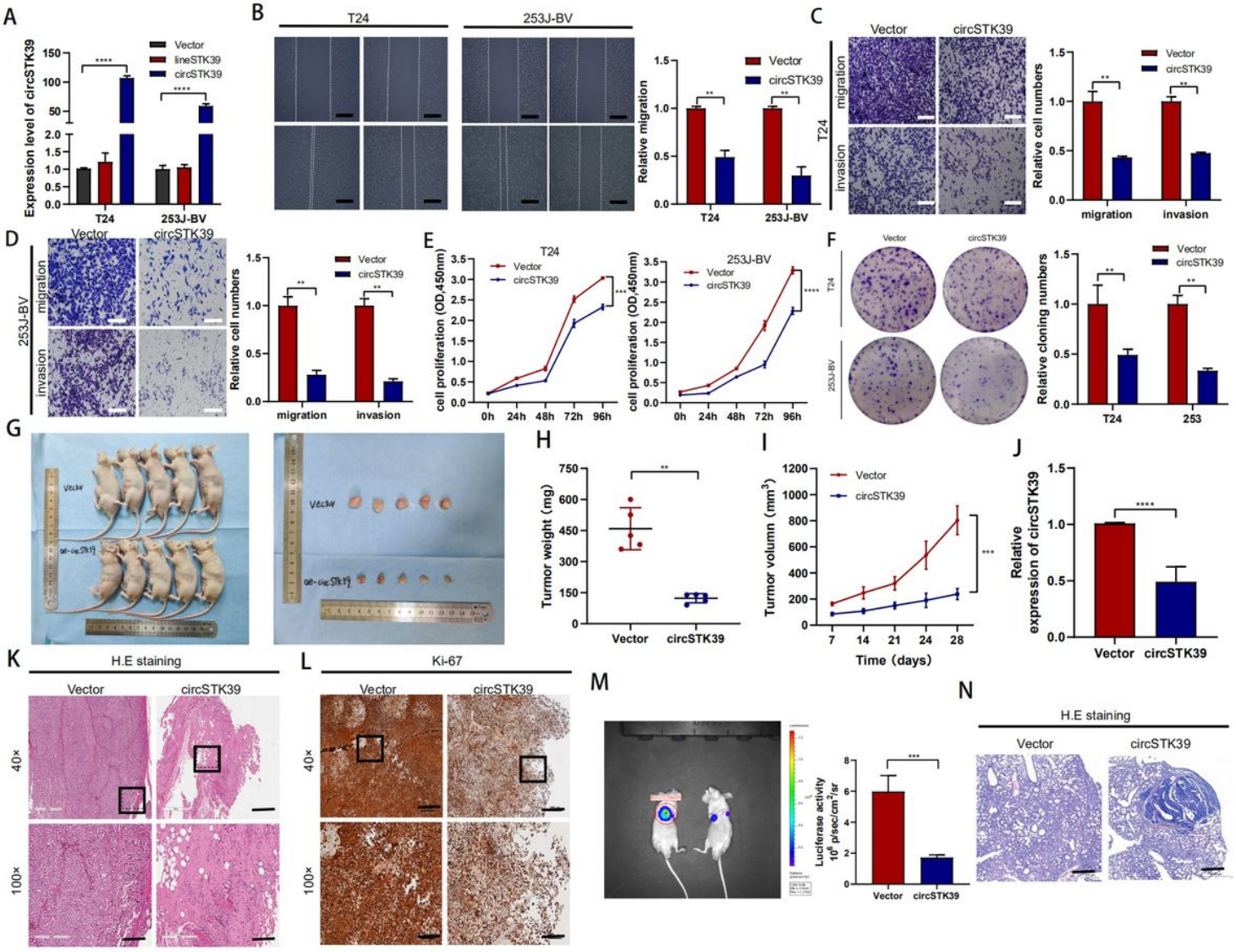

Figure 2

Over-expression of circSTK39 inhibits the proliferation, migration, and invasion of BCa in vitro and in vivo.

(A) After transfection with circSTK39 or control vector plasmids in T24 and 253J-BV cells, the expression of circSTK39 and STK39 mRNA were detected by qRT-PCR.

(B) Effect of overexpression of circSTK39 on cell migration was assessed using wound healing assay.

(C-D) Cell migration and invasion were assessed using transwell assays.

(E-F) Cell growth was assessed using CCK-8 and colony formation assays.

(G) Subcutaneous xenograft tumor models were established by injecting the stably transfected T24 cells with circSTK39 or vector plasmid into BALB/c nude mice (5×10^6 cells per mice, n=5). The representative pictures of xenograft tumor were showed (n=5).

(H-I) The tumor volume and weight were measured weekly and plotted based on the data.

(J) QRT-PCR was performed to detect the expression level of circSTK39.

(K-L) H & E staining was applied to identify the bladder cancer tissues. IHC assay verified the expression level of Ki67 in pairs of bladder cancers.

(M) For lung metastasis model, T24-GFP-luc cells (1×10^6 cells per mice, n=4) into the tail vein of BALB/c nude mice.

(N) H & E staining was applied to identify the metastatic nodules in the lungs.

Data were shown as mean ± SD, n = 3 *P < 0.05, **P < 0.01, ***P < 0.001.

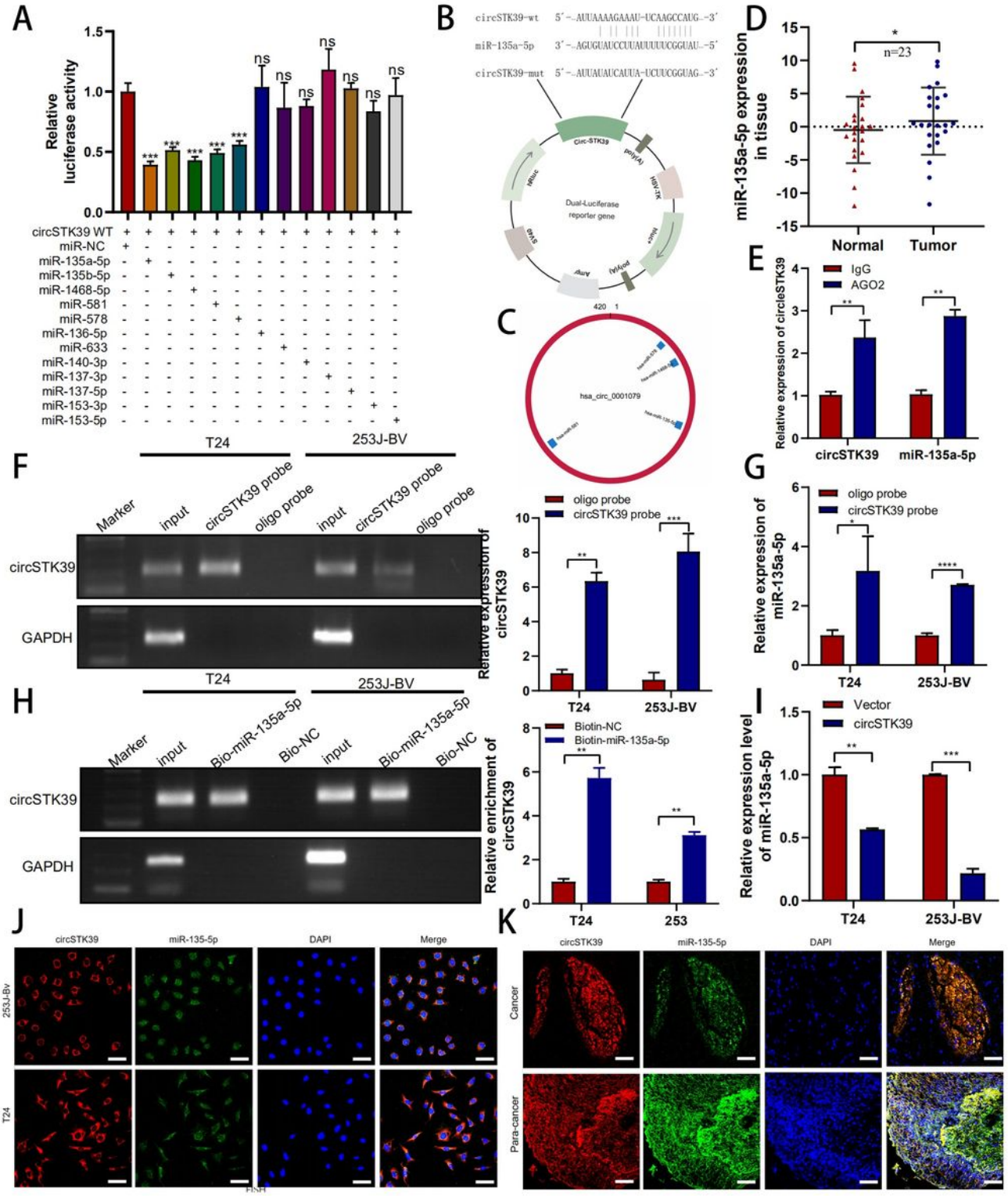

Figure 3

CircSTK39 sponges miR-135a-5p in bladder cancer cells

(A-B) Dual luciferase reporter assay was performed to verify the interaction between circSTK39 and 11 predicted miRNAs in HEK-293T cells. Schematic showed the predicted binding site of miR-135a-5p with circSTK39.

(C) The bioinformation analysis was performed to predict the binding sites between circSTK39

and corresponding miRNAs.

(D) Expression of miR-135a-5p in 23 pairs bladder cancer and normal tissues.

(E) RIP assays were also performed with 5 μg anti-AGO2 antibody or anti-IgG antibody to detect the interaction between circSTK39 and miR-135a-5p.

(F-G) RNA pull-down using a biotin-labeled circSTK39 probe or biotin-labeled oligo probe was

performed to measure the interaction between circSTK39 and miR-135a-5p, and qRT-PCR revealed the expression of circSTK39 and miR-135a-5p.

(H) RNA pull-down using a biotin-labeled miR-135-5p probe or biotin-labeled NC probe was

performed to measure the interaction between circSTK39 and miR-135a-5p, and qRT-PCR revealed the expression of circSTK39.

(I) After overexpression circSTK39, qRT-PCR was used to detect the expression of miR-135a-5p.

(J-K) The co-localization of circSTK39 and miR-135a-5p was presented in bladder tissues (magnification, × 100, Scale bar, 50 μm) and cells (magnification, × 400, Scale bar, 50 μm) by FISH assay.

Data were shown as mean ± SD, n = 3 *P < 0.05, **P < 0.01, ***P < 0.001.

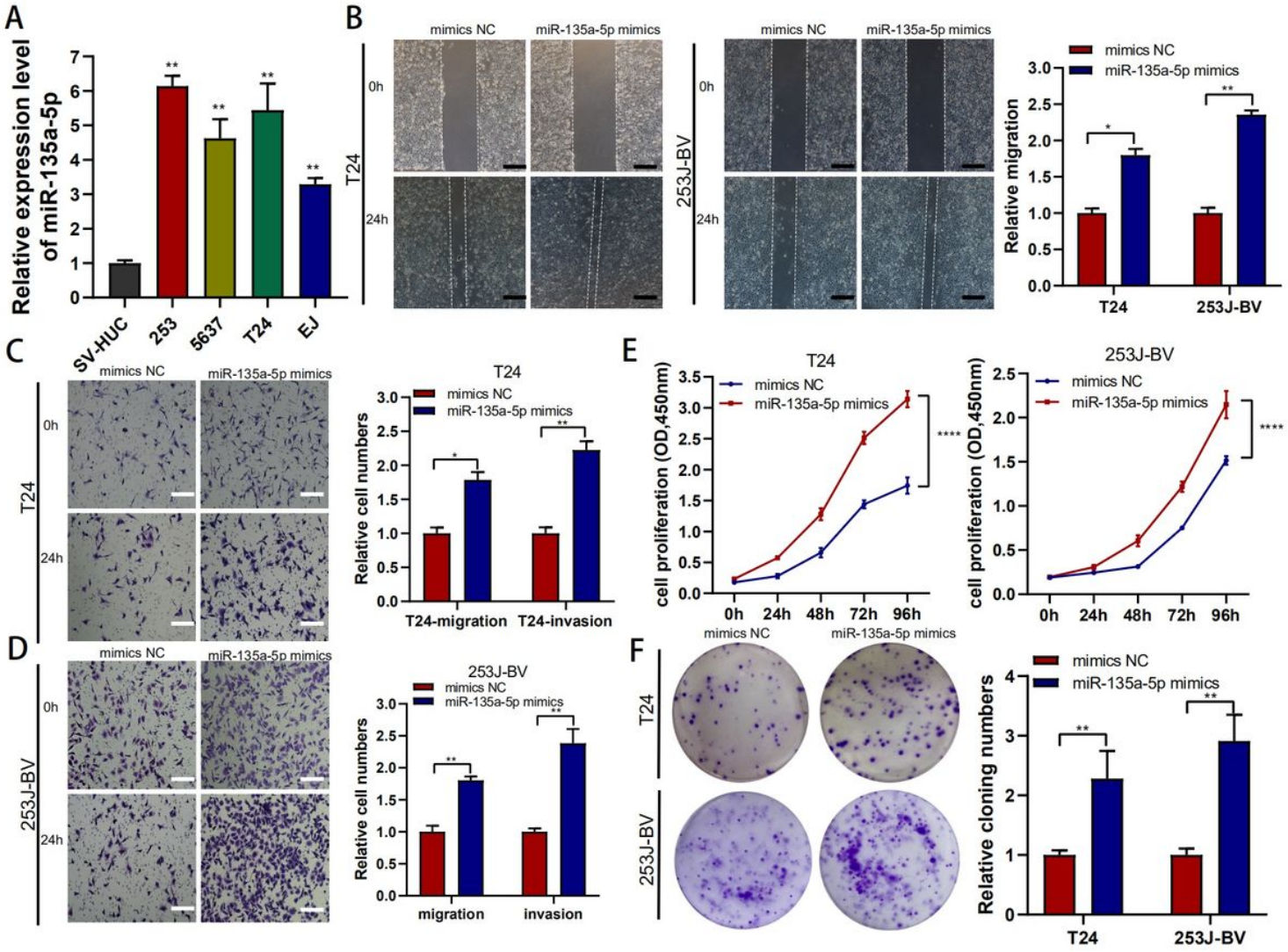

Figure 4

MiR-135a-5p promotes the proliferation, migration, and invasion of bladder cancer cells.

(A) qRT-PCR was used to detect the expression of miR-135a-5p in bladder cancer cells.

(B) Effect of miR-NC mimics or miR-135a-5p mimics on cell migration was assessed using wound healing assay.

(C-D) Cell migration and invasion were assessed using Transwell assays.

(E-F) Cell growth was assessed using CCK-8 and colony formation assays.

Data were shown as mean ± SD, n = 3 *P < 0.05, **P < 0.01, ***P < 0.001.

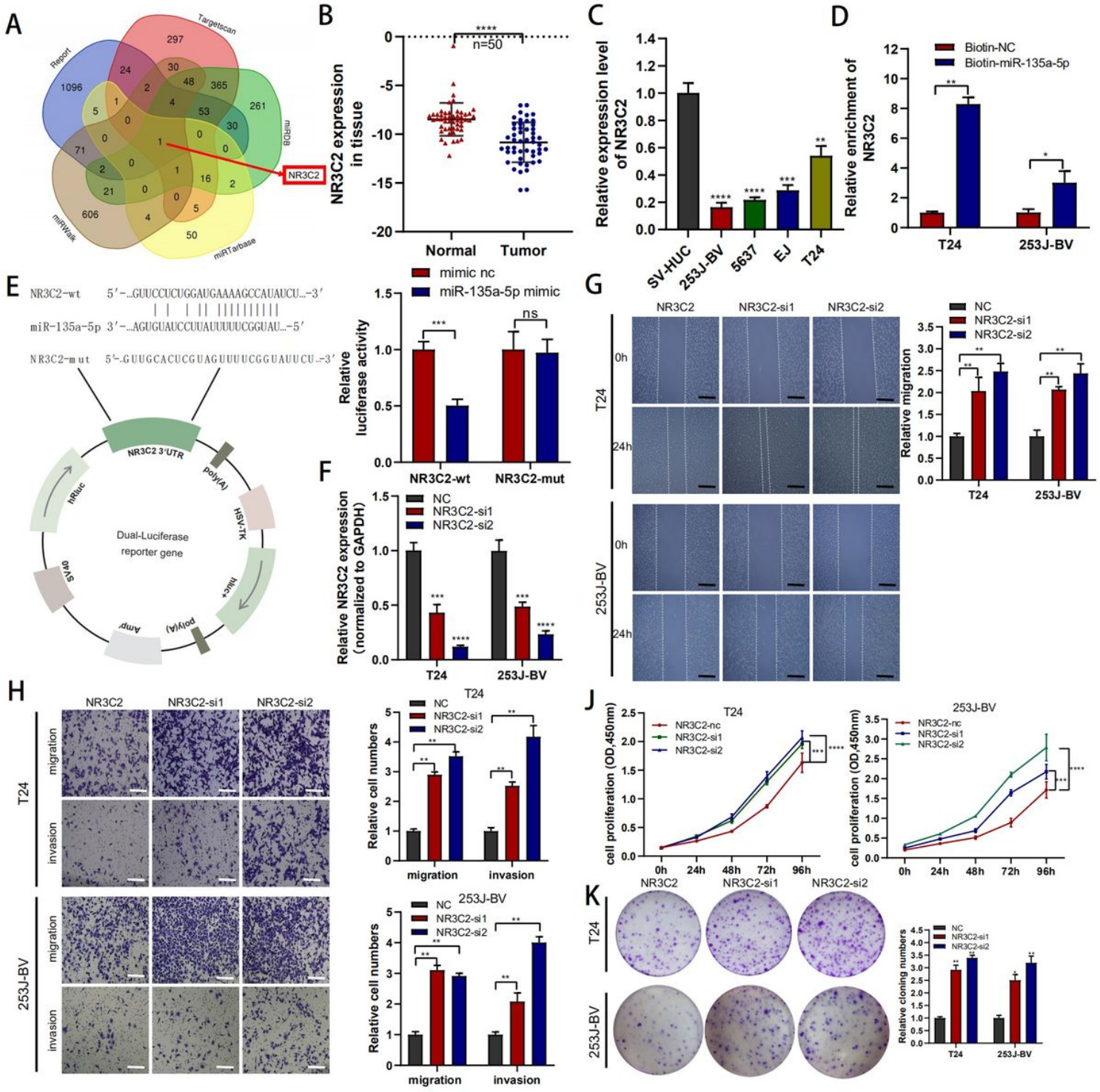

Figure 5

NR3C2 expression is downregulated in bladder cancer cells and tissues

(A) Venn diagram showed that the overlapping of the target gene of miR-135a-5p predicted by five algorithms (Targetscan, miRDB, miRWalk, miRTarbase, and our sequencing resluts) among the downregulated genes.

(B) NR3C2 expression was measured using qRT-PCR in 50 pairs of primary bladder cancer tissues and adjacent normal samples.

(C) NR3C2 expression in SV-HUC-1 and bladder cancer cells were detected by qRT-PCR.

(D) RNA pull-down using a biotin-labeled miR-135a-5p probe or biotin-labeled NC probe was performed to measure the interaction between NR3C2 and miR-135-5p, and qRT-PCR revealed the expression of NR3C2.

(E) Schematic showed the predicted binding site of miR-135a-5p with NR3C2. Dual luciferase reporter assay was performed to verify the interaction between miR-135a-5p and NR3C2 in HEK-293T cells.

(F) After transfection with each siRNA on NR3C2 or control siRNA in T24 and 253J-BV cells, the expression of NR3C2 mRNA were detected by qRT-PCR.

(G) Effect of si NR3C2-1 and si NR3C2-2 on cell migration was assessed using wound healing assay.

(H-I) Cell migration and invasion were assessed using Transwell assays.

(J-K) Cell growth was assessed using CCK-8 and colony formation assays.

Data were shown as mean ± SD, n = 3 *P < 0.05, **P < 0.01, ***P < 0.001.

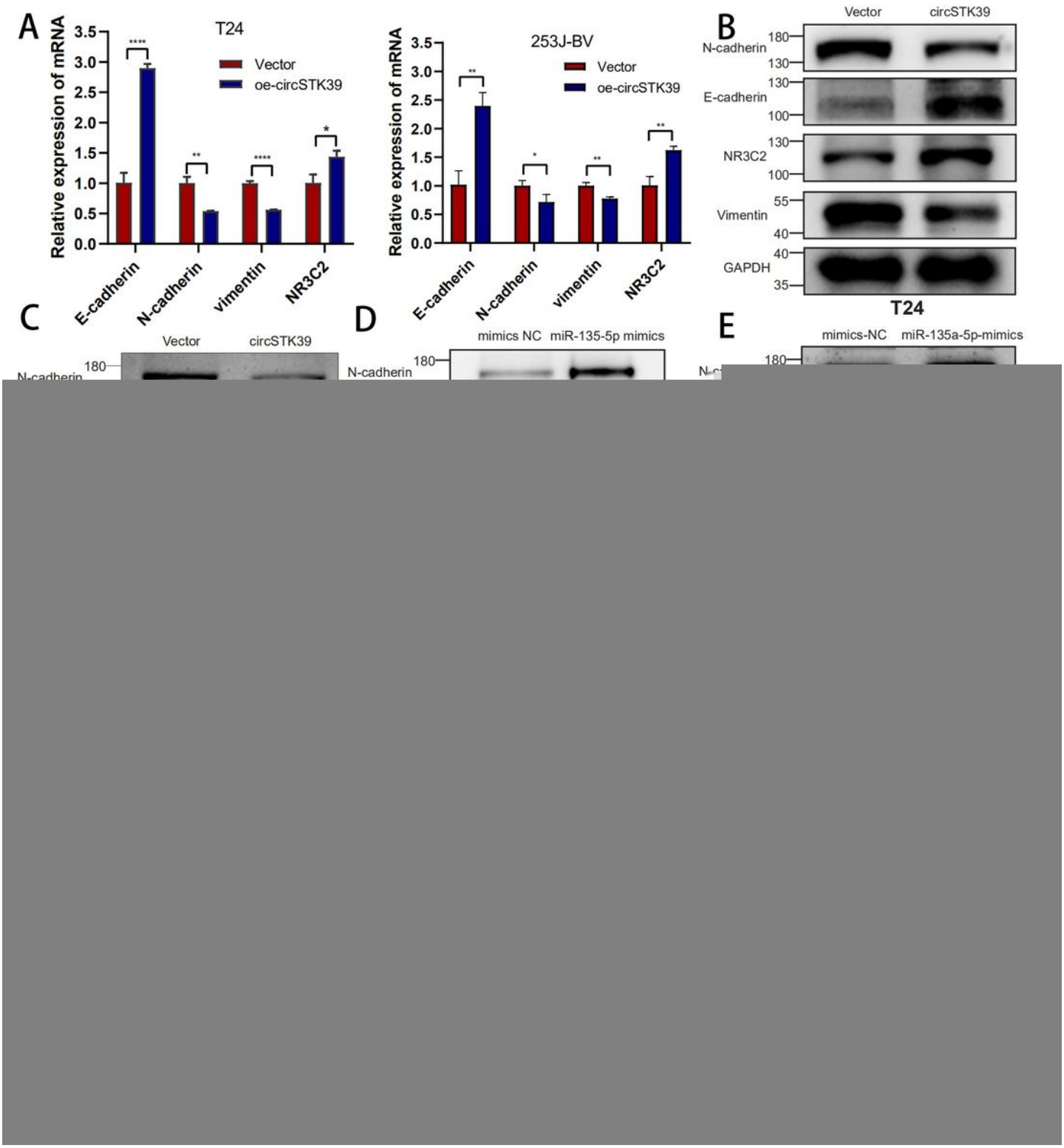

Figure 6

miR-135a-5p could reverse the effects of circSTK39 on bladder cancer cells

(A-C) Effect of overexpression of circSTK39 on the expression level of related mRNAs and proteins in T24 and 253J-BV.

(D-E) Effect of miR-135a-5p mimics on the expression level of related proteins in T24 and 253J-BV.

(F-G) Transwell assays and CCK-8 assays were performed to rescue experiments in T24 and 253J-BV cells to verify whether the inhibitory effect of circSTK39 in bladder cancer cells could be reversed by miR-135-5p.

Data were shown as mean ± SD, n = 3 *P < 0.05, **P < 0.01, ***P < 0.001.

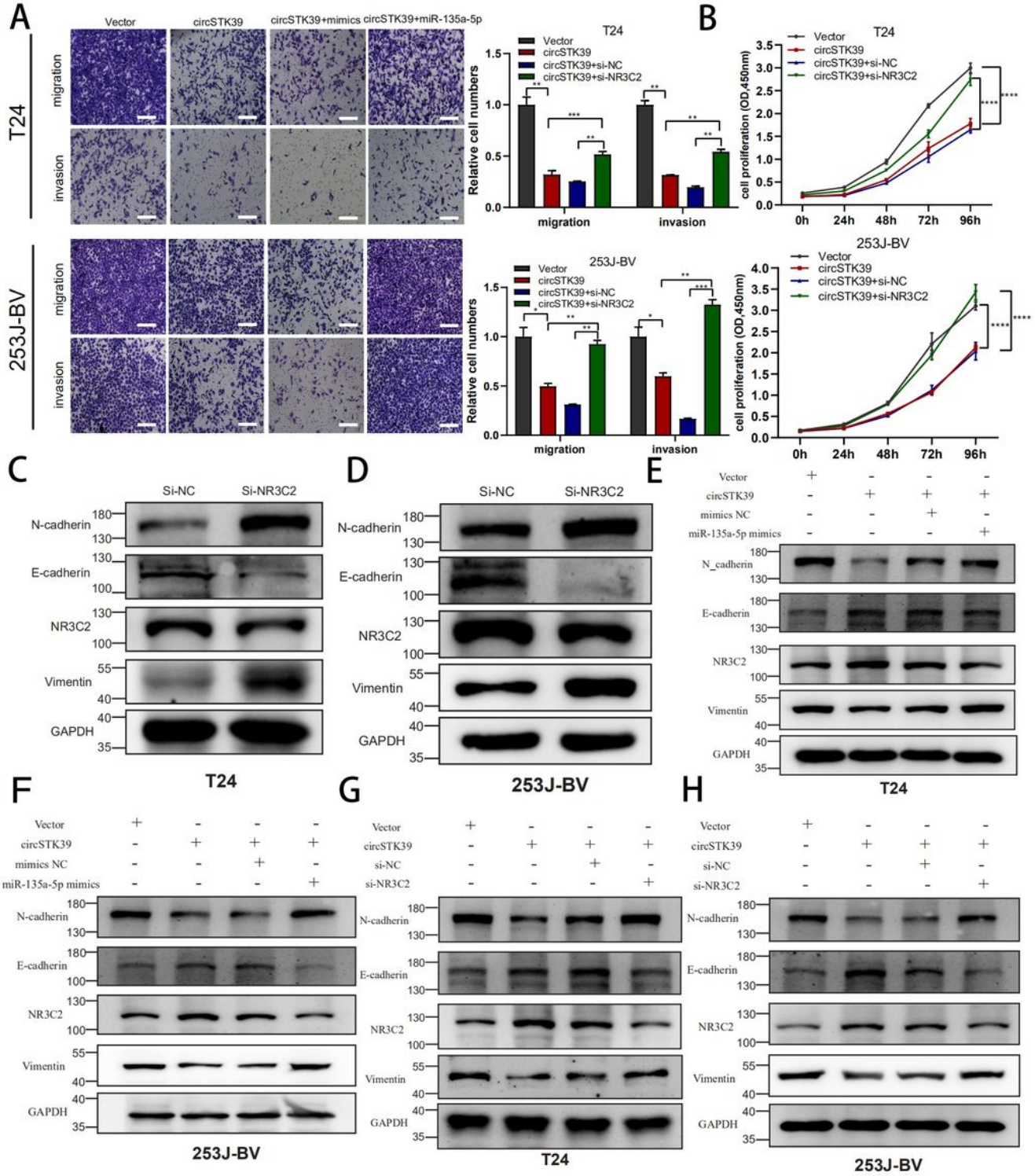

Figure 7

Down-regulated NR3C2 could reverse the effects of circSTK39 on bladder cancer cells

(A-B) Transwell assays and CCK-8 assays were performed to rescue experiments in T24 and 253J-BV cells to verify whether the inhibitory effect of circSTK39 in bladder cancer cells could be reversed by miR-135-5p.

(C-D) Effect of si-NR3C2 on the expression level of related proteins in T24 and 253J-BV.

(E-F) Rescue experiments exhibited that miR-135a-5p could partly inhibit the NR3C2 protein expression levels on the basis of circSTK39 overexpression.

(G-H) Rescue experiments exhibited that si-NR3C2 could partly inhibit the NR3C2 protein expression levels on the basis of circSTK39 overexpression.

Data were shown as mean ± SD, n = 3 *P < 0.05, **P < 0.01, ***P < 0.001.

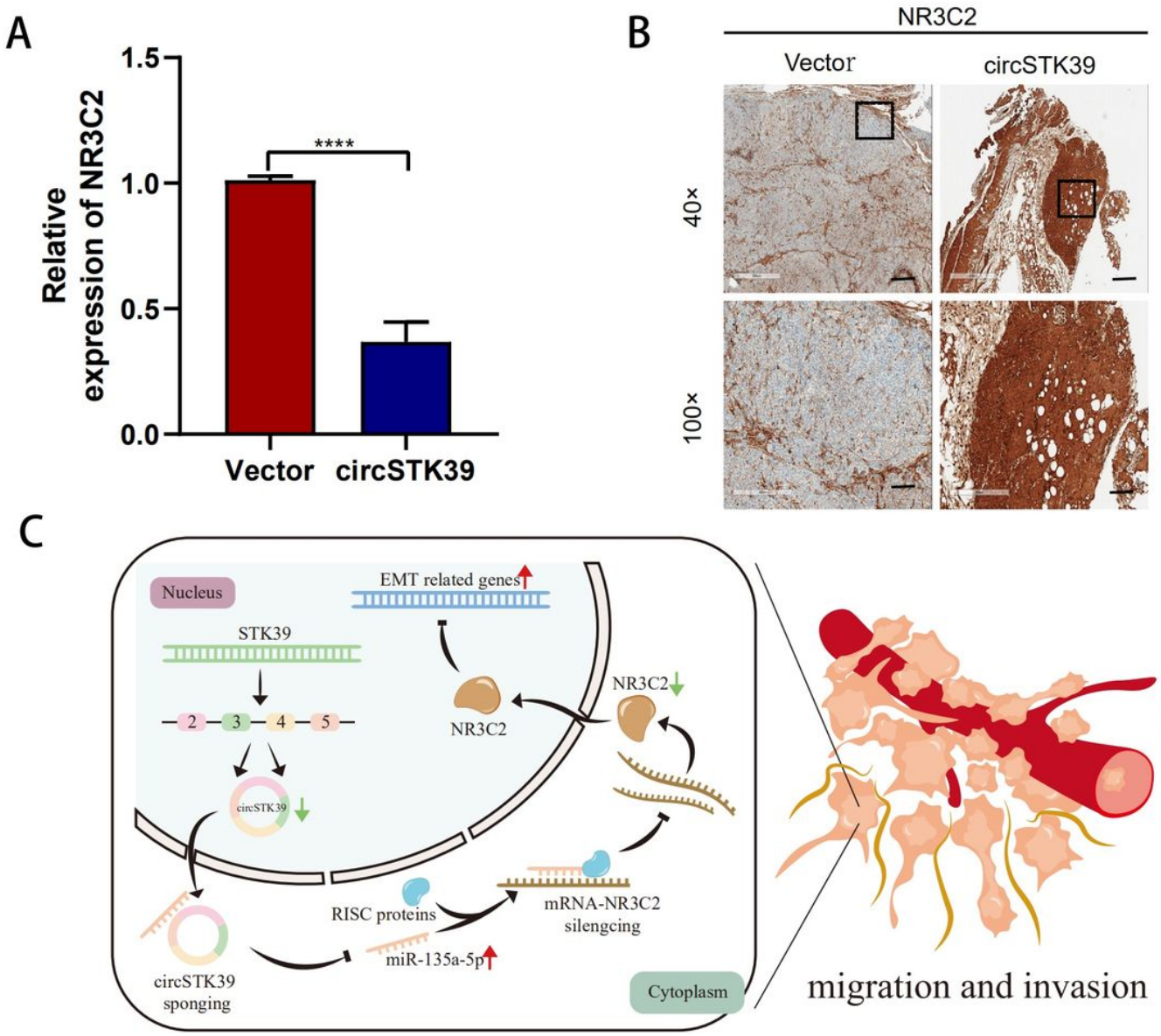

Figure 8

A schematic for the circSTK39/miR-135a-5p/NR3C2/EMT pathway.

(A) QRT-PCR was performed to detect the expression level of NR3C2.

(B) IHC assay verified the expression level of NR3C2 in pairs of bladder cancers.

(C) Schematic illustrating the biological role of the circ_0001079/miR-135a-5p/NR3C2/EMT axis in OS progression and metastasis

Data were shown as mean ± SD, n = 3 *P < 0.05, **P < 0.01, ***P < 0.001.

Supplementary Files

This is a list of supplementary files associated with this preprint. Click to download.

- FigureS100.tif
- FigureS200.tif
- FigureS300.tif
- FigureS400.tif
- TableS1.doc
- TableS2.doc